PNAS
www.pnas.org

Supplementary Information for

Structural evidence for the roles of divalent cations in actin polymerization and activation of ATP hydrolysis.

Clement P. M. Scipion, Umesh Ghoshdastider, Fernando J. Ferrer, Tsz-Ying Yuen, Jantana Wongsantichon & Robert C. Robinson

Robert C. Robinson
Email: rrobinson@imcb.a-star.edu.sg

This PDF file includes:

Figs. S1 to S4
Tables S1 to S3
Captions for movies S1 to S3
Captions for databases S1 to S3
References for SI reference citations

Other supplementary materials for this manuscript include the following:

Movies S1 to S3
Datasets S1 to S3

www.pnas.org/cgi/doi/10.1073/pnas.1806394115

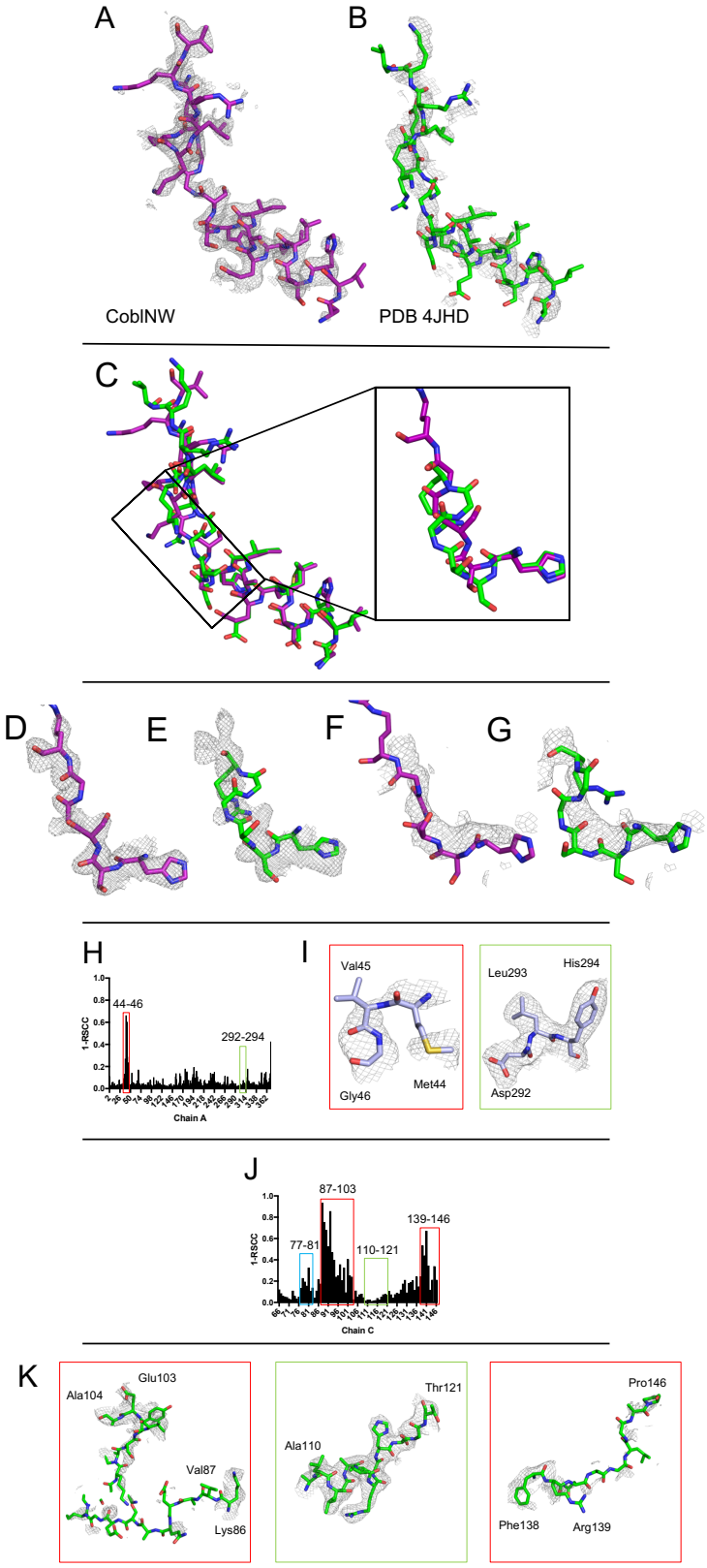

Fig. S1. Comparison of the CoblNW/actin complex with the Cordon-Bleu/actin complex (PDB 4JHD). (*A,B*) The WH2 peptides with their corresponding OMIT maps. (*C*) Alignment of CoblNW with the WH2 portion of Cordon-Bleu, including an enlargement of the divergent portion of the structures. (*D*) The CoblNW structure placed in the CoblNW OMIT map. (*E*) The 4JHD structure placed in the CoblNW OMIT map. (*F*) The CoblNW structure placed in the 4JHD OMIT map. (*G*) 4JHD structure placed in the 4JHD OMIT map. (H,J) 1-RSCC (Real-Space Correlation Coefficient) vs residue of 4JHD chains A and C, respectively. (I,K) Representation of the residues framed in H,J. CoblNW, purple sticks. 4JHD, green sticks (Cordon-Bleu) and light blue sticks (actin). OMIT maps, grey meshes contoured at 0.5 σ (A,B,D-G,I,K). Chain C residues Ser66 – P146 correspond to UniProt accession number Q5NBX1 residues Ser1184 – P1264).

Comment: On superimposing the CoblNW structure onto the PDB 4JHD structure, we observed that the CoblNW structure described the 4JHD electron density better than the 4JHD structure (Fig S1, compare F and G). Therefore, an EDS analysis was performed on 4JHD structure and electron density (1). The real-space correlation coefficient (RSCC) confirmed a divergence between the structure and the density (Fig S1*J*, blue frame and Fig S1*G*). The analysis of the rest of 4JHD showed that the majority of the actin (chain A) exhibited a good structure-to-density correlation (Fig S1*H*), which was confirmed by plotting electron density maps as examples (Fig S1*I*, green frame). Nevertheless, some parts of actin showed poor density, and thus poor RSCC (Fig S1*H,I*, red frames). This corresponds to the DNase I binding loop, which is usually disordered in G-actin structures. Finally, the Cordon-Bleu (chain C) residues 87 to 103, as well as residues 139 to 146, showed no significant electron density (Fig S1*J,K*, red frames). This indicates that the linker between the actin-binding WH2 domains is disordered, as is the ATP cleft-interacting C-terminal tail of the second WH2 domain. Thus, these regions of the 4JHD should not be used for extrapolating biological implications. This analysis corroborates recent studies that re-analysed a Lmod2 polypeptide bridging two WH2 domains (2) for which no electron density was observed for the linker region on re-analysis (3,4).

A

B

Organism	UniProt accession code	Organism	UniProt accession code	Organism	UniProt accession code	Organism	UniProt accession code
Homo sapiens	P60709	*Schizosaccharomyces pombe*	P10989	*Porphyra umbilicalis*	A0A1X6PGF9	*Xenopus tropicalis*	Q6NVA9
Monodelphis domestica	F6RFW8	*Paramecium tetraurelia*	Q867E9	*Noctiluca scintillans*	A7WQ44	*Chlamydomonas reinhardtii*	P53498
Saccharomyces cerevisiae	P60010	*Spironucleus salmonicida*	V6LIA4	*Trichomonas vaginalis*	A2DCC3	*Galdieria sulphuraria*	M2XRF6
Toxoplasma gondii	P53476	*Gallus gallus*	P60706	*Arabidopsis thaliana*	P0CJ46	*Plasmodium falciparum*	P53476
Strongylocentrotus purpuratus	P53473	*Zea mays*	P02582	*Entamoeba histolytica*	P11426	*Monosiga brevicollis*	A9UR87
Danio rerio	Q7ZVI7	*Tetrahymena pyriformis*	P10993	*Neurospora crassa*	P78711	*Dictyostelium discoideum*	P07830
Lokiarchaeum	A0A0F8XG85	*Candidatus Odinarchaeota archaeon*	A0A1Q9N690	*Candidatus Thorarchaeota archaeon*	A0A1Q9NK04	*Candidatus Heimdallarchaeota archaeon*	A0A1Q9NAD8

Fig. S2. The actin amino acid sequence is highly conserved in eukaryotes. (*A*) Sequence Logo of aligned actin sequences from different organisms. Residues indicated by arrows indicate the residues highlighted in Fig. 2. The colours of the arrows match those of the boxes in Fig. 2 (*B*) White background; list of organisms with their respective UniProt access numbers used for alignments showed in (*A*). Grey background; list of Asgard archaea actins that show amino acid conservation in the E57/167 (stiffness), D288/D286/E205 (polymerization), and W356/E631 sites. This suggests an evolutionary conserved role for these sites. (5,6) This suggests an evolutionary conserved role for these sites (5,6). Alignments were performed using Clustal Omega (7) and sequences logo was created using WebLogo (8,9).

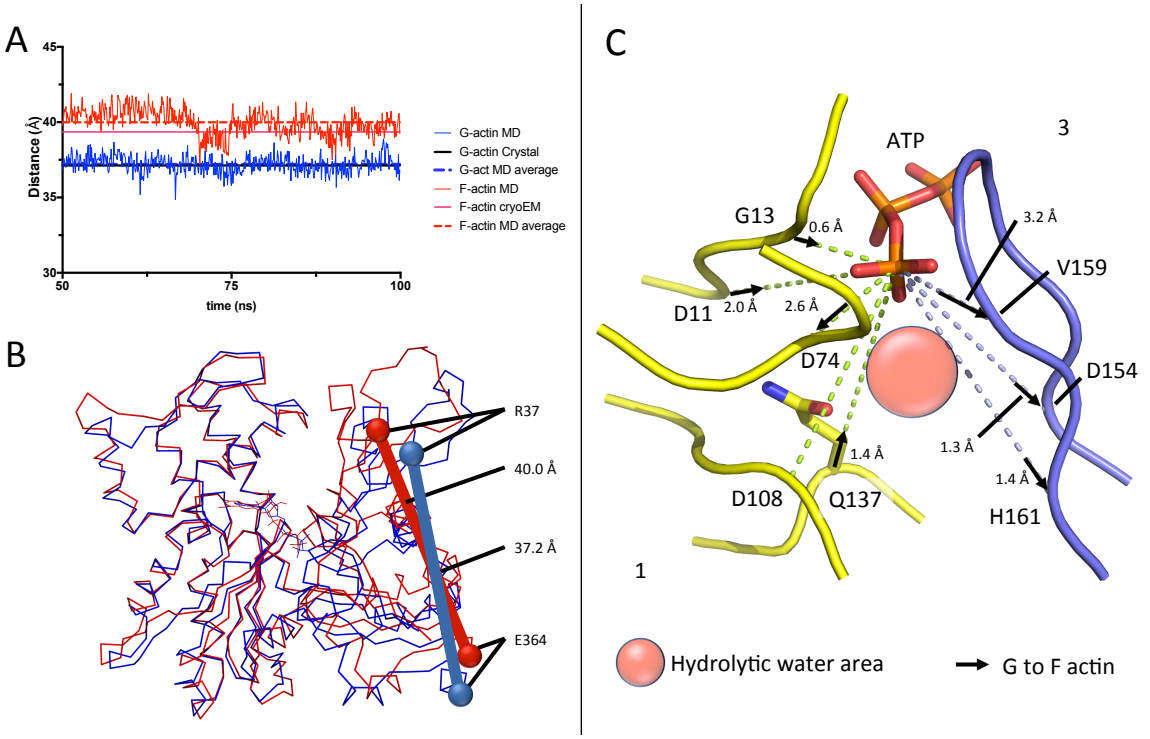

Fig. S3. General analyses of G and F-actin MD simulations. (*A*) Distance between residues 364 (subdomain 1) to 37 (subdomain 2). G-actin crystal, distance in native G-actin crystal structure (PDB accession code 3HBT, (10)). F-actin cryoEM, distance in latest cryoEM structure (PDB accession 5OOE, (11)). (*B*) Superimposition of G and F-actin models used in morphing analysis (Fig 4, Supplementary videos 1, 2 and 3), indicating the distance shown in Fig. S3*A*. The stability of these distances in Fig. S3*A* indicates that G-actin remains G-actin, and F-actin remains F-actin, during the time course of the simulations. (*C*) Movement in residues lining the ATP cleft from the average positions in the G-actin structures to the average positions in the last 50 ns of the F-actin MD simulation under 1 mM $MgCl_2$ and 120 KCl buffer conditions. Subdomain 1, yellow. Subdomain 3, blue.

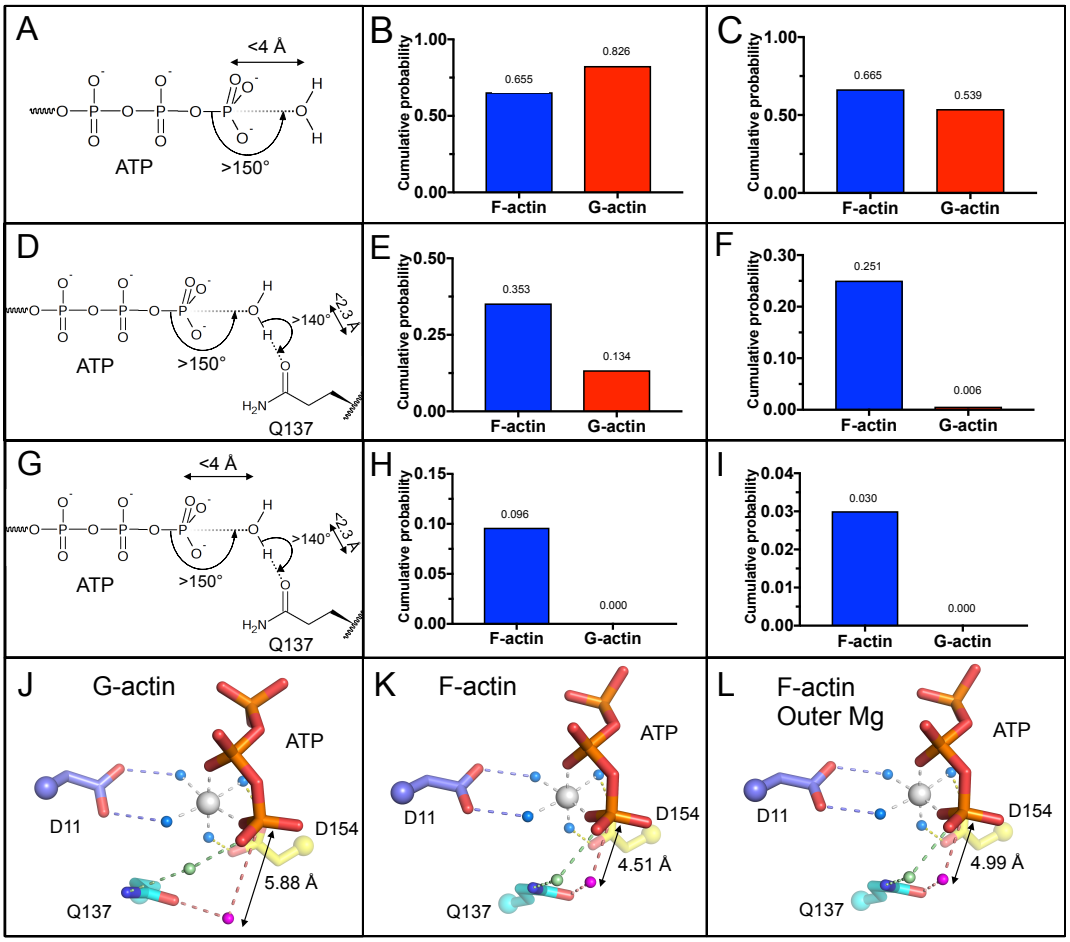

Fig. S4. MD analysis of water molecules close to the ATP γ-phosphorus and Gln137 in high 150 mM $MgCl_2$ conditions. (*A,D,G*) Representation of analysis conditions applied around ATP and Gln137. (*B,C,E,F,H,I*) Cumulative probability of water molecules with applied conditions from *A,D,G*. (*B,E,H*) Starting model included the ATP magnesium ion. (*C,F,I*) Starting model included the ATP magnesium ion and the surface bound magnesium ions from Figure 2, labeled "outer Mg". (J) G-actin model, resulting from the combination of actin-DNaseI structure (PDB accession code 1ATN, (12)) and ATP and ATP-bound magnesium of PDB accession code 2V52 (13). (K,L) Typical snapshots of MD simulation frame satisfying all conditions from (G). ATP and actin, sticks. Water, blue, green and purple spheres. Simulations were performed in 150 mM $MgCl_2$ conditions. Chemical sketches were created using ACD/ChemSketch version 2016.2.2, Advanced Chemistry Development, Inc., Toronto, ON, Canada, www.acdlabs.com.

	Oryctolagus cuniculus Actin−CoblNW‡
Data collection	
Space group	C 2
Cell dimension	
a, b, c (Å)	174.9, 40.8, 109.0
α, β, γ (°)	90.0, 101.8, 90.0
Resolution (Å)	29.8 - 2.0 (2.07 - 2.00)*
Rmerge (%)	11.3 (52.2)*
Rmeas (%)	13.3 (63.0)*
Mean I/sigma(I)	7.6 (1.4)*
Completeness (%)	97 (98)*
Redundancy	3.6 (3.1)*
CC1/2	0.995 (0.806)*
Refinement	
No. of reflections	50,252 (4,115)*
Rwork/Rfree	19.9/24.2 (27.7/29.6)*
No. of atoms	
Actin	5,601
mCoblNle-WH2	334
ATP, Ca^{2+}	62, 7
Waters	615
B factors (Å^2)	
Actin/mCoblNle-WH2	29.5
ATP, Ca^{2+}	19.1
Water	35.3
RMSD	
Bonds (Å)	0.010
Angles (°)	1.40
Molprobity statistics	
Clashscore, all atoms	3.31
Poor rotamers (%)	1.42
Ramachandran outliers (%)	0.0
Ramachandran favored (%)	97.97
Molprobity score	1.24 (99th percentile)
Cβ deviations > 0.25Å (%)	0.0
Bad backbone bonds (%)	0.0
Bad backbone angles (%)	0.0

‡ PDB ID code 5YPU

* Values in parentheses are for the highest resolution shell

Table S1. Data collection and refinement statistics. Each crystallographic asymmetric unit contains 2 copies of the complex. The ordered residues of actin comprise amino acids Thr5-Gly36 and Ser52-Arg372, consistent with other reported actin crystal structures, where the N-terminus (residues 1-4) and DNase I binding loop (residues 37-51) are disordered and the C-terminus (residues 373-375) is sometimes not observed. The ordered region of the WH2-motif peptide comprises the entire peptide (Ser1184-Val1205).

Number	PDB ID	Site identified	Actin	Ligand	Cation	Nucleotide	Resolution (Å)	Ref
1	4PKH	E167	Alpha skeletal muscle	Nterm Tropomodulin-1 Gelsolin chimera	Ca^{2+}	ADP	2.15	(14)
2	4PKI	E167	Alpha skeletal muscle	Cterm Tropomodulin-1 Gelsolin chimera	Ca^{2+}	ATP	2.3	(14)
3	4CBU	E167	Plasmodium falciparum actin I	Gelsolin	Ca^{2+}	ATP	1.3	(15)
4	4CBW	E167	Plamodium berghei I with D-loop from muscle actin	Gelsolin	Ca^{2+}	ATP	2.5	(15)
5	4K41	Q263/S265	Alpha skeletal muscle	Kabimaride C	Ca^{2+}	ATP	1.4	(16)
6	1T44	E167	Alpha skeletal muscle	Chimera of Gelsolin G1 and C-term Tb4	Ca^{2+}	ATP	2.0	(17)
7	1MDU	E167	Chicken actin	Gelsolin G1	Ca^{2+}	ATP	2.2	(18)
8	4CBX	E167	Plasmodium berghei actin II	Gelsolin	Ca^{2+}	ATP	2.2	(15)
9	3M6G	E205, Q354/W356/E361, V30	Alpha skeletal muscle	Lobophorolide	Mg^{2+}	ATP	2.0	(19)
10	2HMP	E125, E125/N128, V30	Alpha skeletal muscle	Cleaved with ECP32	Sr^{2+}	ATP	1.9	(20)
11	2VYP	D286/D288, E167, Q354/W356/E361	Alpha skeletal muscle	Myxobacterial rhizopodin	Ca^{2+}	ATP	2.32	(21)
12	1EFH	S271	Acanthamoeba actin	Spir domain D	Ca^{2+}	ADP	2.48	(22)
13	1C0G	E167	Dictyostelium/Tetrahymena chimera actin	Gelsolin G1	Ca^{2+}	ATP	2.0	(23)
14	1DEJ	E167	Dictyostelium/Tetrahymena chimera actin	Gelsolin G1	Ca^{2+}	ATP	2.4	(23)
15	1EQY	E167	Alpha skeletal muscle	Gelsolin G1	Ca^{2+}	ATP	2.3	(24)
16	1C0F	E167	Dictyostelium actin	Gelsolin G1	Ca^{2+}	ATP	2.4	(23)
17	3A5O	E167	Dictyostellium actin	Gelsolin G1	Ca^{2+}	ATP	2.4	(25)
18	3A5N	E167	Dictyostellium actin	Gelsolin G1	Ca^{2+}	ATP	2.36	(25)
19	2FF6	E167	Alpha skeletal muscle	Gelsolin G1, Ciboulot D2	Ca^{2+}	ATP	2.05	(26)
20	1ESV	E167	Alpha skeletal muscle	Gelsolin G1, Latrunculin	Ca^{2+}	ATP	2.0	(27)
21	2FF3	E167	Alpha skeletal muscle	Nterm WASP V2	Ca^{2+}	ATP	2.0	(26)
22	3A5L	E167	Dictyostellium actin	Gelsolin G1	Mg^{2+}	ADP	2.4	(25)
23	3UB5	S199/T201/E205	Cow cytoplasmic 1	Profilin (open)	Ca^{2+}	ATP	2.2	(28)
24	3U4L	D288	Cow cytoplasmic 1	Profilin	Ca^{2+}	ATP	2.4	(28)
25	2FXU	Q263/S265 & D286/D288	Alpha skeletal muscle	Bistramide A	Ca^{2+}	ATP	1.35	(29)
26	1J6Z	E205 & Q354/W356/E361	Alpha skeletal muscle	Rhodamine	Ca^{2+}	ADP	1.54	(30)
27	2ASP	Q263/S265	Alpha skeletal muscle	Reidispongiolide C	Ca^{2+}	ATP	1.64	(31)
28	2ASM	Q263/S265	Alpha skeletal muscle	Reidispongiolide A	Ca^{2+}	ATP	1.6	(31)
29	2Q0R	Q263/S265	Alpha skeletal muscle	Pectenotoxin-2	Ca^{2+}	ATP	1.7	(32)
30	2Q0U	Q263/S265	Alpha skeletal muscle	Pectenotoxin-2, Latrunculin B	Ca^{2+}	ATP	1.45	(32)
31	2HF3	Q263/S265	Drosophilia Actin 5C		Ca^{2+}	ADP	1.8	(33)
32	3EKS	Q263/S265	Drosophilia Actin 5C	Cytochalasin D	Ca^{2+}	ATP	1.8	(34)
33	1NWK	Q263/S265 & Q354/W356/E361	Alpha skeletal muscle		Ca^{2+}	AMPNP	1.85	(35)
34	2HF4	Q263/S265	Drosophilia Actin 5C		Ca^{2+}	ATP	1.8	(33)
35	3EKU	Q263/S265	Drosophilia Actin 5C	Cytochalasin D	Ca^{2+}	ATP	2.5	(34)
36	3EL2	Q263/S265	Drosophilia Actin 5C	Anti-parallel dimmer	Ca^{2+}	ATP	2.5	(34)
37	2A5X	Q263/S265	Alpha skeletal muscle	Cross-linked actin dimer	Ca^{2+}	AMPNP	2.49	(36)
38	4Z94	E167/G90/D85	Alpha skeletal muscle	Tropomodulin-1 and Leiomodin-1 chimera	Ca^{2+}	ATP	2.4	(37)
39	5UBO	E167	Mical oxidized Alpha skeletal muscle	Gelsolin G1	Ca^{2+}	ATP	2.39	(38)
40	5YPU	D187, D286/D288, D363	Alpha skeletal muscle	Cordon-Bleu MET1190NLE WH2-motif peptide	Ca^{2+}	ATP	2.0	-

Table S2. Actin crystal structures reveal G-actin bound divalent cations

PDB ID	Cation	Nucleotide	Resolution (Å)	13Cα	11Cα	137Cα	108Cα	74Cα	161Cα	159Cα	154Cα	$137O_E$
4PKI	Ca^{2+}	ATP	2.3	4.59	9.87	9.7	8.44	5.06	9.29	5.09	7.90	6.09
4CBU	Ca^{2+}	ATP	1.3	4.58	9.84	9.69	8.36	5.12	9.33	5.13	8.17	6.12
4CBW	Ca^{2+}	ATP	2.5	4.62	9.65	9.59	8.12	5.15	9.20	5.35	7.99	5.7
4K41	Ca^{2+}	ATP	1.4	4.61	9.90	9.45	8.34	5.17	9.36	5.07	8.07	5.93
1T44	Ca^{2+}	ATP	2.0	4.59	9.89	9.6	8.45	5.15	9.57	5.18	8.17	6.06
1MDU	Ca^{2+}	ATP	2.2	4.62	9.95	9.78	8.4	5.29	9.32	5.12	8.06	6.15
1MDU	Ca^{2+}	ATP	2.2	4.54	10.02	9.82	8.43	5.25	9.31	4.96	8.05	6.28
4CBX	Ca^{2+}	ATP	2.2	4.63	9.94	9.85	8.49	5.16	8.97	5.10	8.13	6.16
3M6G	Mg^{2+}	ATP	2.0	4.78	9.92	10.19	8.28	5.31	9.12	5.07	7.97	5.91
3M6G	Mg^{2+}	ATP	2.0	4.74	8.77	9.51	8.17	5.22	9.22	5.20	8.09	5.97
2HMP	Sr^{2+}	ATP	1.9	4.66	10.06	9.97	8.54	5.27	9.30	5.36	8.08	6.49
2HMP	Sr^{2+}	ATP	1.9	4.64	9.97	9.85	8.45	5.17	9.42	5.23	8.15	6.39
2VYP	Ca^{2+}	ATP	2.32	4.52	9.79	9.28	8.13	5.19	9.40	5.15	8.03	5.84
2VYP	Ca^{2+}	ATP	2.32	4.82	10.05	9.60	8.28	5.38	9.21	5.21	7.79	6.12
1C0G	Ca^{2+}	ATP	2.0	4.46	9.82	9.61	8.28	5.12	9.38	5.14	8.2	5.92
1DEJ	Ca^{2+}	ATP	2.4	4.59	9.88	9.63	8.33	5.16	9.40	5.17	8.18	5.95
1EQY	Ca^{2+}	ATP	2.3	4.53	9.78	9.50	8.56	5.22	9.51	5.01	8.15	5.68
1C0F	Ca^{2+}	ATP	2.4	4.63	9.97	9.69	8.35	5.10	9.34	5.09	8.22	6.11
3A5O	Ca^{2+}	ATP	2.4	4.59	10.00	9.93	8.52	5.12	9.49	5.07	8.14	6.12
3A5N	Ca^{2+}	ATP	2.36	4.54	9.96	9.89	9.13	5.16	9.33	5.04	8.15	6.28
2FF6	Ca^{2+}	ATP	2.05	4.57	9.84	9.59	8.28	5.06	9.38	5.06	8.13	6.05
1ESV	Ca^{2+}	ATP	2.0	4.47	9.63	9.54	8.37	4.92	9.45	5.03	8.18	6.02
2FF3	Ca^{2+}	ATP	2.0	4.53	9.90	9.75	8.36	5.14	9.35	5.13	8.08	6.25
3UB5	Ca^{2+}	ATP	2.2	5.39	11.33	11.17	9.36	5.58	10.88	6.58	9.88	7.91
3U4L	Ca^{2+}	ATP	2.4	4.37	9.49	9.17	7.97	5.36	9.34	5.66	7.95	5.56
2FXU	Ca^{2+}	ATP	1.35	4.61	9.85	9.49	8.30	5.07	9.36	5.10	8.05	5.96
2ASP	Ca^{2+}	ATP	1.64	4.60	9.91	9.86	7.25	5.12	9.47	5.22	8.18	5.98
2ASM	Ca^{2+}	ATP	1.6	4.65	9.92	9.47	8.37	5.15	9.37	5.15	8.11	6.04
2Q0R	Ca^{2+}	ATP	1.7	4.51	9.77	9.37	8.32	5.16	9.46	5.20	8.15	5.83
2Q0U	Ca^{2+}	ATP	1.45	4.52	9.76	9.26	8.22	5.11	9.51	5.19	8.14	5.69
3EKS	Ca^{2+}	ATP	1.8	4.50	9.80	9.66	8.51	5.19	9.55	5.40	8.37	6.88
2HF4	Ca^{2+}	ATP	1.8	4.63	9.99	9.69	8.43	5.33	9.40	5.26	8.14	6.08
3EKU	Ca^{2+}	ATP	2.5	4.65	9.91	9.71	8.30	5.49	9.40	5.21	8.27	6.62
3EL2	Ca^{2+}	ATP	2.5	4.56	9.88	9.75	8.26	5.44	9.33	5.17	8.13	6.83
4Z94	Ca^{2+}	ATP	2.4	4.51	9.77	9.53	8.41	5.04	9.30	5.11	8.03	6.16
5UBO	Ca^{2+}	ATP	2.39	4.55	9.85	9.63	8.37	5.06	9.39	5.06	8.00	6.04
			AVERAGE	**4.61**	**9.88**	**9.69**	**8.36**	**5.19**	**9.40**	**5.20**	**8.15**	**6.14**
F-actin MgOuter MD (1mM $MgCl_2$, 120mM KCl)	Mg^{2+}	ATP	-	**4.00**	**7.86**	**8.30**	**8.35**	**7.13**	**11.28**	**8.43**	**9.45**	**5.17**
			DIFFERENCE	**0.61**	**2.02**	**1.39**	**0.01**	**-1.94**	**-1.88**	**-3.23**	**-1.3**	**0.97**

Table S3. Distances in G-actin crystal structures from ATP Pγ to different atoms. AVERAGE, average of distances in crystal structures. DIFFERENCE, difference between the crystal structure average and the MD average distances.

Movie S1. Morphing from G to F-actin, overall view. Actin subdomains 1 and 2, light blue ribbons. Actin subdomains 3 and 4, yellow ribbons. Actin subdomains 1 and 3 interface α-helix, cyan cartoon. ATP, sticks. Magnesium, grey sphere. The MD initial model was used for G-actin. For F-actin, a typical snapshot of an MD frame bearing all the conditions from Fig. 4E was selected. The LSQMAN software package was used to generate the morphs (http://xray.bmc.uu.se/usf/).

Movie S2. Morphing from G to F-actin, overall side-view. Actin subdomains 1 and 2, light blue ribbons. Actin subdomains 3 and 4, yellow ribbons. Actin subdomains 1 and 3 interface α-helix, cyan cartoon. ATP, sticks. Magnesium ion, grey sphere.

Movie S3. Morphing from G to F-actin, close-up around ATP. ATP, sticks. Magnesium ion, grey sphere. Asp11, light blue sticks. Gln137, cyan sticks. Asp154, yellow sticks. Water, blue, green and purple spheres.

Additional Dataset PDB S1 (separate file)

Initial model for the F-actin MD simulations including ATP and magnesium ions.

Additional Dataset PDB S2 (separate file)

F-actin after completion of the MD simulation (t=0 ns). Conditions of 1 mM $MgCl_2$ and 120 mM KCl were used.

Additional Dataset PDB S3 (separate file)

F-actin after completion of the MD simulation (t=100 ns). Conditions of 1 mM $MgCl_2$ and 120 mM KCl were used.

References

1. Kleywegt GJ, Harris MR, Zou JY, Taylor TC, Wählby A, Jones TA. The Uppsala Electron-Density Server. Acta Crystallogr Sect D Biol Crystallogr. 2004;60(12 I):2240–9.
2. Chen X, Ni F, Kondrashkina E, Ma J, Wang Q. Mechanisms of leiomodin 2-mediated regulation of actin filament in muscle cells. Proc Natl Acad Sci [Internet]. 2015;112(41):12687–92. Available from: http://www.pnas.org/lookup/doi/10.1073/pnas.1512464112
3. Boczkowska M, Yurtsever Z, Rebowski G, Eck MJ, Dominguez R. Crystal Structure of Leiomodin 2 in Complex with Actin: A Structural and Functional Reexamination. Biophys J. 2017;113(4):889–99.
4. Pollard TD. A Third Look at the Structure of Leiomodin Bound to Actin. Vol. 113, Biophysical Journal. 2017. p. 762–4.
5. Spang A, Saw JH, Jørgensen SL, Zaremba-Niedzwiedzka K, Martijn J, Lind AE, et al. Complex archaea that bridge the gap between prokaryotes and eukaryotes. Nature. 2015;521(7551):173–9.
6. Zaremba-Niedzwiedzka K, Caceres EF, Saw JH, Bäckström Di, Juzokaite L, Vancaester E, et al. Asgard archaea illuminate the origin of eukaryotic cellular complexity. Nature. 2017;541(7637):353–8.
7. Sievers F, Wilm A, Dineen D, Gibson TJ, Karplus K, Li W, et al. Fast, scalable generation of high-quality protein multiple sequence alignments using Clustal Omega. Mol Syst Biol. 2011;7.
8. Schneider TD, Stephens RM. Sequence logos: A new way to display consensus sequences. Nucleic Acids Res. 1990;18(20):6097–100.
9. Crooks GE, Hon G, Chandonia JM, Brenner SE. WebLogo: A sequence logo generator. Genome Res. 2004;14(6):1188–90.
10. Wang H, Robinson RC, Burtnick LD. The structure of native G-actin. Cytoskeleton. 2010;67(7):456–65.
11. Merino F, Pospich S, Funk J, Wagner T, Küllmer F, Arndt H-D, et al. Structural transitions of F-actin upon ATP hydrolysis at near-atomic resolution revealed by cryo-EM. Nat Struct Mol Biol [Internet]. 2018; Available from: https://www.nature.com/articles/s41594-018-0074-0.pdf%0Ahttp://www.nature.com/articles/s41594-018-0074-0
12. Kabsch W, Mannherz HG, Suck D, Pai EF, Holmes KC. Atomic structure of the actin:DNase I complex. Nature. 1990 Sep;347(6288):37–44.
13. Mouilleron S, Guettler S, Langer CA, Treisman R, McDonald NQ. Molecular basis for G-actin binding to RPEL motifs from the serum response factor coactivator MAL. EMBO J. 2008;27(23):3198–208.
14. Rao JN, Madasu Y, Dominguez R. Mechanism of actin filament pointed-end capping by tropomodulin. Science (80-) [Internet]. 2014;345(6195):463–7. Available from: http://www.sciencemag.org/cgi/doi/10.1126/science.1256159
15. Vahokoski J, Bhargav SP, Desfosses A, Andreadaki M, Kumpula EP, Martinez SM, et al. Structural Differences Explain Diverse Functions of Plasmodium Actins. PLoS Pathog. 2014;10(4).
16. Pereira JH, Petchprayoon C, Hoepker AC, Moriarty NW, Fink SJ, Cecere G, et al. Structural and biochemical studies of actin in complex with synthetic macrolide tail analogues. ChemMedChem. 2014;9(10):2286–93.
17. Irobi E, Aguda AH, Larsson M, Guerin C, Yin HL, Burtnick LD, et al. Structural basis of actin sequestration by thymosin-β4: implications for WH2 proteins. EMBO J [Internet]. 2004;23(18):3599–608. Available from: http://emboj.embopress.org/cgi/doi/10.1038/sj.emboj.7600372
18. Dawson JF, Sablin EP, Spudich JA, Fletterick RJ. Structure of an F-actin trimer disrupted by gelsolin and implications for the mechanism of severing. J Biol Chem. 2003;278(2):1229–38.
19. Blain JC, Mok YF, Kubanek J, Allingham JS. Two molecules of lobophorolide cooperate to stabilize an actin dimer using both their “ring” and “tail” region. Chem Biol. 2010;17(8):802–7.
20. Klenchin VA, Khaitlina SY, Rayment I. Crystal Structure of Polymerization-Competent Actin. J Mol Biol. 2006;362(1):140–50.
21. Hagelueken G, Albrecht SC, Steinmetz H, Jansen R, Heinz DW, Kalesse M, et al. The absolute configuration of rhizopodin and its inhibition of actin polymerization by dimerization. Angew Chemie - Int Ed. 2009;48(3):595–8.
22. Pedersen LC, Petrotchenko E V., Negishi M. Crystal structure of SULT2A3, human hydroxysteroid sulfotransferase. FEBS Lett. 2000;475(1):61–4.

23. Matsuura Y, Stewart M, Kawamoto M, Kamiya N, Saeki K, Yasunaga T, et al. Structural basis for the higher Ca2+-activation of the regulated actin-activated myosin ATPase observed with Dictyostelium/Tetrahymena actin chimeras11Edited by A. Klug. J Mol Biol [Internet]. 2000;296(2):579–95. Available from: http://www.sciencedirect.com/science/article/pii/S0022283699934678
24. McLaughlin PJ, Gooch JT, Mannherz H-G, Weeds AG. Structure of gelsolin segment 1-actin complex and the mechanism of filament severing. Nature [Internet]. 1993;364(6439):685–92. Available from: http://www.nature.com/doifinder/10.1038/364685a0
25. Murakami K, Yasunaga T, Noguchi TQP, Gomibuchi Y, Ngo KX, Uyeda TQP, et al. Structural Basis for Actin Assembly, Activation of ATP Hydrolysis, and Delayed Phosphate Release. Cell. 2010;143(2):275–87.
26. Aguda AH, Xue B, Irobi E, Préat T, Robinson RC. The Structural Basis of Actin Interaction with Multiple WH2/β-Thymosin Motif-Containing Proteins. Structure [Internet]. 2017 Sep 24;14(3):469–76. Available from: http://dx.doi.org/10.1016/j.str.2005.12.011
27. Morton WM, Ayscough KR, McLaughlin PJ. Latrunculin alters the actin-monomer subunit interface to prevent polymerization. Nat Cell Biol. 2000;2(6):376–8.
28. Porta JC, Borgstahl GEO. Structural basis for profilin-mediated actin nucleotide exchange. J Mol Biol. 2012;418(1–2):103–16.
29. Rizvi SA, Tereshko V, Kossiakoff AA, Kozmin SA. Structure of bistramide A-actin complex at a 1.35 ?? resolution. J Am Chem Soc. 2006;128(12):3882–3.
30. Otterbein LR. The Crystal Structure of Uncomplexed Actin in the ADP State. Science (80-) [Internet]. 2001;293(5530):708–11. Available from: http://www.sciencemag.org/cgi/doi/10.1126/science.1059700
31. Allingham JS, Zampella A, D'Auria MV, Rayment I. Structures of microfilament destabilizing toxins bound to actin provide insight into toxin design and activity. Proc Natl Acad Sci U S A [Internet]. 2005;102(41):14527–32. Available from: http://www.pnas.org/search?tmonth=&pubdate_year=2005&submit=yes&submit=Submit&submit=yes&andorexacttitle=and&format=standard&firstpage=14527&fmonth=&title=&tyear=&hits=10&titleabstract=&volume=102&sortspec=relevance&andorexacttitleabs=and&author2=&tocsect
32. Allingham JS, Miles CO, Rayment I. A Structural Basis for Regulation of Actin Polymerization by Pectenotoxins. J Mol Biol. 2007;371(4):959–70.
33. Rould MA, Wan Q, Joel PB, Lowey S, Trybus KM. Crystal structures of expressed non-polymerizable monomeric actin in the ADP and ATP states. J Biol Chem. 2006;281(42):31909–19.
34. Nair UB, Joel PB, Wan Q, Lowey S, Rould MA, Trybus KM. Crystal Structures of Monomeric Actin Bound to Cytochalasin D. J Mol Biol. 2008;384(4):848–64.
35. Graceffa P, Dominguez R. Crystal structure of monomeric actin in the ATP state: Structural basis of nucleotide-dependent actin dynamics. J Biol Chem. 2003;278(36):34172–80.
36. Kudryashov DS, Sawaya MR, Adisetiyo H, Norcross T, Hegyi G, Reisler E, et al. The crystal structure of a cross-linked actin dimer suggests a detailed molecular interface in F-actin. Proc Natl Acad Sci U S A [Internet]. 2005;102(37):13105–10. Available from: http://www.pnas.org/content/102/37/13105
37. Boczkowska M, Rebowski G, Kremneva E, Lappalainen P, Dominguez R. How Leiomodin and Tropomodulin use a common fold for different actin assembly functions. Nat Commun [Internet]. 2015;6(May):8314. Available from: http://www.nature.com/doifinder/10.1038/ncomms9314
38. Grintsevich EE, Ge P, Sawaya MR, Yesilyurt HG, Terman JR, Zhou ZH, et al. Catastrophic disassembly of actin filaments via Mical-mediated oxidation. Nat Commun. 2017;8(1).